

## [Impact of roughness on shock wave reflection phenomena]

Thomas LECHAT<sup>(1)</sup> \*, Sébastien OLLIVIER<sup>(2)</sup>, Didier DRAGNA<sup>(1)</sup>, Maria KARZOVA<sup>(1, 3)</sup>

<sup>(1)</sup>Univ Lyon, Ecole Centrale de Lyon, INSA Lyon, Université Claude Bernard Lyon I, CNRS, LMFA, UMR 5509,  
36 Avenue Guy de Collongue, F-69134, ECULLY, France

<sup>(2)</sup> Univ Lyon, Université Claude Bernard Lyon I, Ecole Centrale de Lyon, INSA Lyon, CNRS, LMFA, UMR 5509,  
43 boulevard du 11 novembre 1918, F-69100, VILLEURBANNE, France

<sup>(3)</sup>Faculty of Physics, M. V. Lomonosov Moscow State University, Moscow 119991, Russia

### Abstract

Reflection of pressure shock waves on a flat surface can lead to a 3-shock reflection pattern, called Mach reflection, with reference to Ernst Mach, who provided evidence for this non-linear interaction [1]. This phenomenon has been widely studied in cases of supersonic jets and high-amplitude pressure generated by moving supersonic bodies or blast waves. In the case of weak shocks (Mach number  $< 1.3$ ), 3-shock(s) reflection patterns are also observed, and in particular in the case of acoustic shock waves. If the irregular reflection of shocks on a flat surface is well known, the effects of roughness have been much less studied. In this work we performed numerical simulation of shock propagation over periodic and random surfaces and compared results to experiments. Numerical simulations are based on the temporal integration of axi-symmetric curvilinear Euler equations. Simulations are compared to Schlieren visualizations of the reflection of spark generated N-waves over sandpaper. The results show that near a rough surface, the pressure level is higher than in the case of a flat surface and the pressure decrease above the surface is also changed. The method will also be applied at larger scales, for example for sonic boom or blast waves reflection over the ground.

Keywords: Physical acoustics, shock wave

## 1 INTRODUCTION

Several applications, such as reduction of sonic boom noise annoyance, pyrotechnics and chemistry industry, or explosion safety, are connected to the prediction of shock wave propagation and reflection. Contrary to linear acoustics, shock waves can interact to form complex reflection pattern when the grazing angle is sufficiently small. The Mach reflection, named after the pioneer work of Ernst Mach, occurs when the incident and reflected shocks interact to form a third shock perpendicular to the surface. The intersection point of these three shocks is named the triple point. This phenomenon was an important subject of research during the last century and is now well known for flat surfaces. To make a step forward in shock wave prediction, it is necessary to account for more complex surfaces, especially roughness or topographic effects. In the case of large scale shock waves due to supersonic aircraft or thunder, it is expected that wave diffraction over hills, buildings or trees change the shock wave pattern and the reflected shock strength [2]. Experimental work from T. Adachi *et al* [3] investigated the reflection of shock waves over a multi-guttered wedge as a first step to dust layer model. When the incident shock propagates over the surface, compression and rarefaction waves are diffracted from the surface and interact with one other to constitute the reflected shock. Depending of the surface geometry, the triple point trajectory can change and the triple shock pattern can disappear for sufficiently large roughness.

Few simulations of the reflection of weak shock waves over irregular surface have been achieved to predict shock wave behavior, especially for weak shocks waves. For example, reflection on curved surfaces has been recently studied to predict the behavior of aerodynamic strong shocks [9]. It is worth mentioning that roughness is already known to perturb the dynamic of the fluid for shock wave propagation inside ducts: the position of

\*corresponding author, thomas.lechat@ec-lyon.fr

the transition from deflagration to detonation of gas explosion inside the channel changes with the roughness of the duct walls [10].

The main goal of this work is to numerically study the impact of the roughness on the pressure field with a particular interest to the separation between the coherent and the incoherent part of the field. For this, simulations are performed for 20 realizations of the rough surface. The roughness characteristics are chosen to be close to standard sandpapers named P40 and P80. This paper follows comparison between simulations and measurements performed at laboratory scale [4].

The paper is organized as follows. Sec. 2 presents the numerical tools used to simulate shock wave propagation and reflection over an irregular surface. In Sec. 3, the shock reflection pattern for rough surfaces is analyzed and compared to that of a smooth surface. Waveforms obtained from the 20 realizations of the rough surface are examined and coherent and incoherent parts of the signals are discussed. Finally, an extension to the study of sonic boom reflection on an irregular terrain is considered in Sec. 4.

## 2 METHOD

In this section, we first describe the configuration of shock wave the reflection we want to simulate. Then, numerical tools are recalled for the sake of completeness.

### 2.1 Problem statement

The configuration and numerical tools are identical to those employed in our precedent work [4]. Irregular reflection occurs when the shock wave is sufficiently strong and at grazing angle. The acoustic source used for experiments presented in Ref. [4] was an electrical spark that generates shock waves of a few kPa. The spark was located at  $h_s = 2.1$  cm from the surface as shown in Fig. 1. The same parameters are taken for the present numerical study.



Figure 1. Experiment configuration: the source is located at  $h_s = 2.1$  cm from the surface (or from the mean height of the roughness).

The surface profiles for the simulations are randomly generated. The autocorrelation function of the surface height is Gaussian, with standard deviations set to to  $66 \mu\text{m}$  and  $129 \mu\text{m}$  for P80 and P40, respectively and correlation length set to  $181 \mu\text{m}$  and  $337 \mu\text{m}$  for P80 and P40, respectively. Paper P40 has then the biggest roughness and paper P80 the smallest one. These parameters were measured on sandpaper samples with a digital microscope VHX-6000 (Keyence, USA). Simulations are performed at laboratory scale to be easily compared to our previous work.

### 2.2 Numerical tools

The axisymmetric Euler equations are solved using high order finite difference time domain algorithm developed initially for computational aeroacoustic applications [11]. The source is an initial overpressure with a Gaussian envelope, centered at  $h_s = 2.1$  cm from the surface. The maximum overpressure is set to  $7.5$  kPa and the half-

width of the Gaussian is set to 2.5 mm. These parameters have been obtained from a comparison in free field with measured pressure signals generated by an electrical spark source.

High order finite-difference schemes optimized to reduce dispersion and dissipation are used to evaluate spatial derivatives. For the interior points, centered schemes are used. For the boundary points, non-centered schemes are employed, except near the axisymmetric boundary for which the symmetry of the fields allows the use of centered schemes. This increases accuracy in the region near the source where the overpressure is maximum. Time integration is performed using a low-storage optimized 4th order Runge Kutta algorithm. Two different filters are applied at each time step to ensure stability: a selective filter to remove grid-to-grid oscillations and a shock capturing filter applied only near the shocks and dedicated to reduce high frequency components generated at the shocks that are not resolved by the numerical schemes [12].

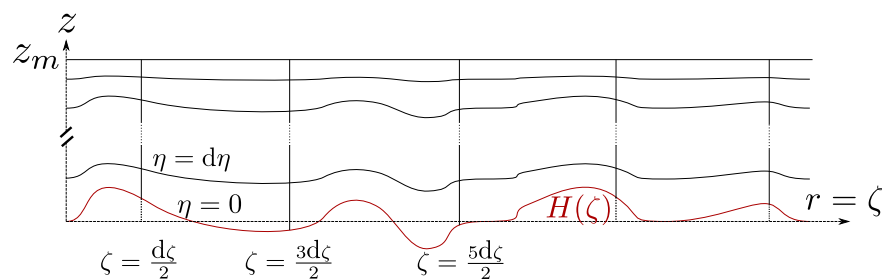


Figure 2. Coordinate system used to describe roughness in time domain simulations.

All these tools have been successfully used to describe shock wave propagation over a flat surface at grazing angle [8]. Extension to non-flat surface is here done. For this, curvilinear coordinates are introduced. The idea is to define a mapping from a Cartesian grid  $(r, z)$  to a body-fitted grid  $(\zeta, \eta)$  as presented in Fig. 2. All partial derivatives are then expressed in this new coordinate system. This approach has already been used for linear acoustic wave propagation in the atmosphere above an irregular terrain [7]. The mapping is here defined by:

$$r = \zeta,$$

$$z = \eta \left( \frac{z_m - H(\zeta)}{z_m} \right) + H(\zeta),$$

where  $H(\zeta)$  corresponds to the surface height and  $z_m$  is the maximum elevation of the computational domain. The mesh deformation is maximum at the surface and is gradually reduced up to the top of the domain. This approach has some advantages compared to other existing methods. It does not require interpolation contrary to, for instance, immersed boundary conditions. The use of a curvilinear coordinate system is also relevant for nonlinear wave propagation because high order finite difference methods still apply without modification. The main drawback is the mesh generation which is not straightforward for complex geometries.

Concerning the boundary conditions, the normal velocity at the surface is null and non-reflection boundary conditions are implemented at the other boundaries. A moving window is also used to reduce the computational cost. The time step is set to  $dt = 0.25 \times 10^{-7}$  s and spatial steps are respectively equal to  $d\zeta = 0.025$  mm and  $d\eta = 0.05$  mm which corresponds to CFL (Courant–Friedrichs–Lewy) number equal to 0.34 and 0.17 respectively.

### 3 RESULTS

We performed 20 simulations for both sets of parameters P40 and P80 in order to be able to separate the coherent part (obtained by ensemble-averaging) from the incoherent part (obtained by subtracting the coherent part to the signal).

### 3.1 Pressure fields and waveforms

Reflection patterns of one realization for both roughness (P40 and P80) and for the smooth reference surface are presented in Fig. 3. The pressure field is plotted at 33 cm from the source up to  $z = 4.5$  cm. The height of the Mach stem resulting from the interaction of the incident and reflected shocks is highlighted with a black dotted line. For the smooth surface, it is about 2 cm. For rough surfaces, it is smaller and it can be seen that the Mach stem height decreases with increasing roughness size. For both P40 and P80, a diffracted field is visible behind the front shock. It consists of small amplitude waves that are continuously generated as the incident wave propagates along the rough surface. The characteristics of these waves (amplitude and spatial scale) are correlated to roughness parameters because they change between P40 and P80.

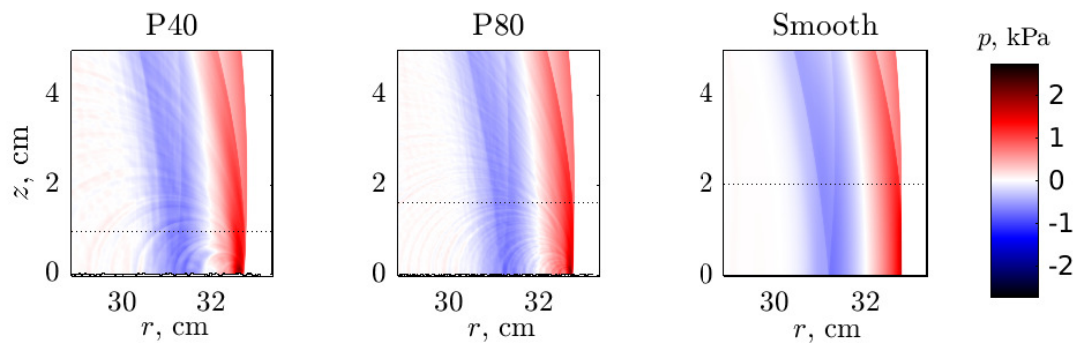


Figure 3. Pressure fields obtained from simulation with P40 paper, P80 paper and smooth surface. Mach stem height is indicated with a black dotted line on each pictures.

In Fig. 4, the pressure waveforms obtained from the twenty realizations of the rough surface P40 are plotted both at  $z = 2$  mm and  $z = 45$  mm from the surface and at  $r = 33$  cm from the source. At  $z = 2$  mm, incident and reflected shocks converge near the surface to form the Mach stem. The maximum pressure obtained on the Mach stem at  $940 \mu\text{s}$  varies with the realization of the rough surface. On the opposite, at  $z = 35$  mm, the incident and reflected shocks are dissociated. The incident shock at  $940 \mu\text{s}$  is therefore the same for all realizations. The reflected shock changes with the surface realization, but the variation of its amplitude is smaller than that observed near the surface for the Mach stem.

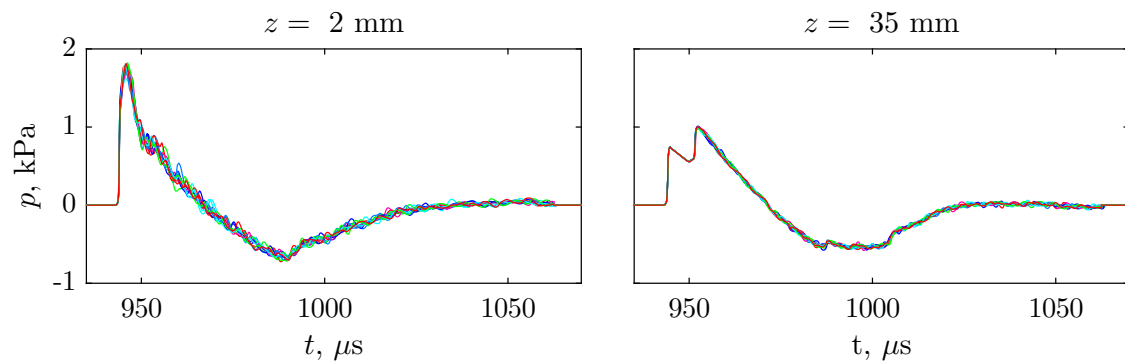


Figure 4. Waveforms of pressure at  $r = 33$  cm and  $z = 2$  mm (left) or  $z = 35$  mm (right) for 20 realizations of the roughness with P40 parameters.

### 3.2 Near surface pressure

In Fig. 5, the average maximum pressure  $\langle p_{\max} \rangle$  over the 20 realizations at  $r = 33$  cm from the source is plotted as a function of the height above the surface. Below  $z = 5$  mm, the maximum overpressure for both P40 and P80 is greater than that of the smooth surface: the roughness induces a higher maximum overpressure in this configuration. The decrease with height also changes. For a smooth surface, the pressure along the Mach stem is almost constant. But in case of a rough surface, the decrease of the pressure with height is rather exponential. This difference suggests the presence of a surface wave propagating along the surface, as it is the case for linear electromagnetic waves propagating over rough resistive surfaces [5] or as it was recently highlighted in linear acoustics by Faure *et al.* [6].

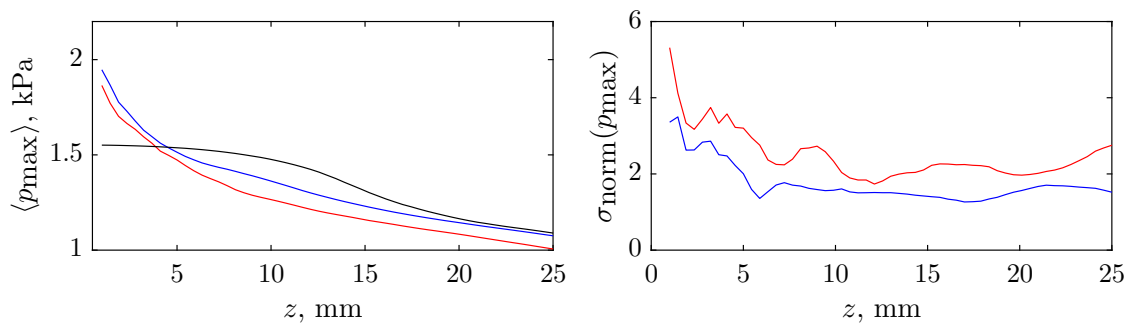


Figure 5. (left) Average maximum overpressure over the 20 realization of the surface roughness as a function of the height above the surface: — P40, — P80 and — smooth reference surface. (right) Normalized standard deviation of the maximum overpressure expressed in percent as a function of the height above the surface.

The normalized standard deviation of the maximum overpressure  $\sigma_{\text{norm}}$  is also plotted in Fig. 5. It never exceeds 10 percent, and stays near 2.5 percent past 5 mm. This value of the standard deviation shows that the incoherent part of the waveform is small compared to the coherent part. Therefore, if measurement uncertainties are of the same order than uncertainties related to the incoherent fluctuations, this confirms that numerical results from a single realization of a rough surface can be compared successfully to experimental results, as it has been done in Karzova *et al.* [4].

### 3.3 Coherent waveforms

Another way to observe the impact of the roughness on pressure waveforms is to look at the average or coherent waveforms  $\langle p \rangle$ . They are obtained by ensemble-averaging of the waveforms obtained from the 20 realizations of the rough surface. The coherent waveforms at  $r = 33$  cm and  $z = 2$  mm are shown in Fig. 6. The maximum pressure is higher for rough surfaces than for the smooth surface as expected. The rise time of the front shock is also longer when the roughness increases in size. Almost all the oscillations on the negative parts of the signal, which can be seen in Fig. 4, disappear: they are strongly dependent of the surface profile and are smoothed out by ensemble averaging. Corresponding spectra are plotted in Fig. 6. They are almost identical below 20 kHz. Above this frequency, the roughness induces two modifications of the spectra compared to a smooth surface. First, an increase of the pressure level can be seen on a frequency band, which depends on the roughness parameters. It is between 25 kHz and 100 kHz for P40 and between 40 kHz and 200 kHz for P80. Second, at higher frequencies, the levels are reduced and decrease more rapidly with frequency.

Figure 7 shows incoherent waveforms for 3 realizations of the rough surfaces. They have been obtained by subtracting the coherent part to the waveforms. Their amplitude is quite low compared to that of the coherent part as expected regarding Fig. 3. The corresponding energy spectral density (ESD) is plotted in Fig. 7. It is retrieved that the levels of the incoherent part are very small compared to that of the coherent waveforms.

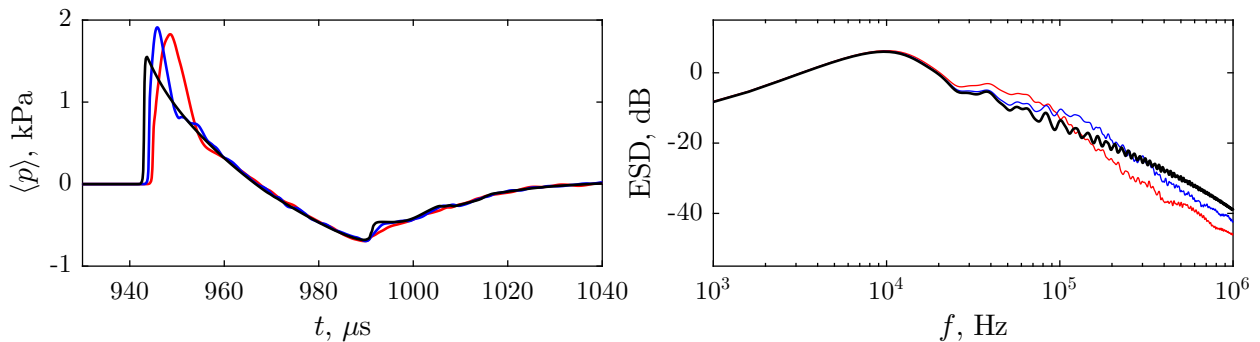


Figure 6. (left) Coherent pressure signal at  $r = 33$  cm from the source and  $z = 2$  mm: — P40, — P80 and — smooth surface reference. (right) Corresponding spectra of the coherent waveforms. The dB reference is  $4.10^{-10} \text{ Pa}^2 \text{ s}^2$ .

Maxima of the spectra coincide with the local maxima observed on coherent spectra.

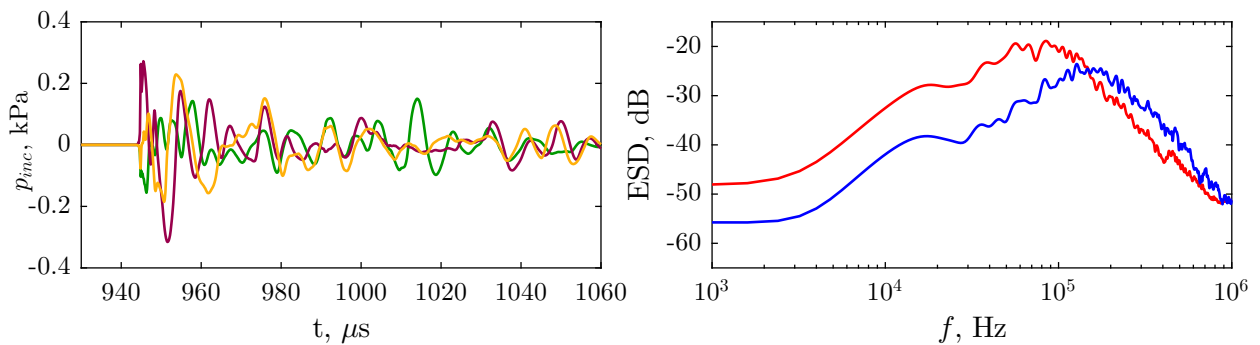


Figure 7. (left) Incoherent pressure signal at  $r = 33$  cm from the source for  $z = 2$  mm and for 3 realizations of paper P40 are plotted. (right) Mean spectra of the incoherent signals obtained from ensemble averaging over the 20 realizations: — P40, — P80. The dB reference is  $4.10^{-10} \text{ Pa}^2 \text{ s}^2$ .

#### 4 FEASIBILITY STUDY OF SONIC BOOM REFLECTION

One application where shock wave reflection occurs is sonic boom level prediction. In Fig. 8, a snapshot of the pressure field obtained with a preliminary 2D simulation of sonic boom propagation over a rough surface is plotted. The incident wave is a  $N$ -wave with an amplitude of 100 Pa and a length of 100 m. This configuration corresponds to a shock wave generated by a supersonic civil aircraft of the first generation, like the Concorde. The source moves at Mach 1.4. The size of the ground roughness is of the order of a hilly terrain. Diffracted waves appear behind the front shock as expected from the small scale simulations. For this incident pressure and incidence angle, no Mach stem is visible.

Some effects described above could occur, especially the higher overpressure on the ground with roughness compared to the flat surface case. Futur works will deal with realistic ground parameters and the effects on low-boom waveforms.

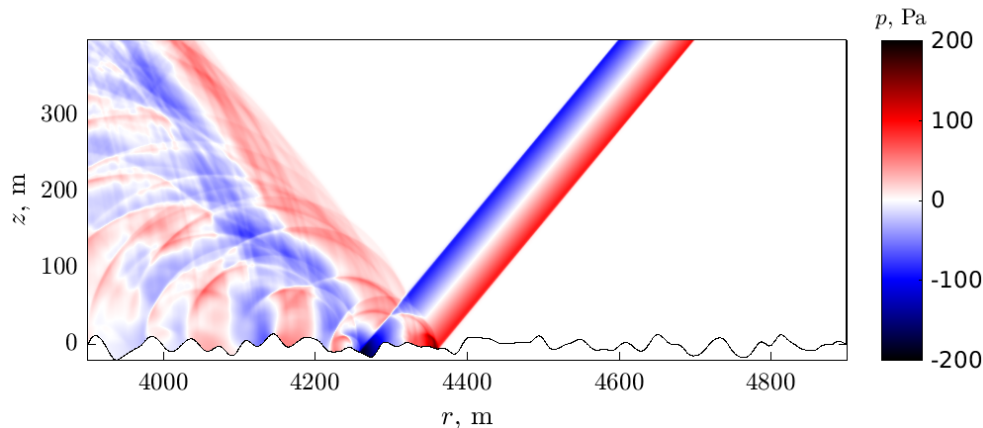


Figure 8. Example of a snapshot of the pressure field for a simulation of a N-wave propagating along a rough surface at sonic boom scale.

## 5 CONCLUSION

Time domain finite difference simulations were used to investigate reflection of weak shock waves over rough surfaces. Roughness was accounting for in simulation by transforming the Euler equations with a curvilinear coordinate system. Two abrasive paper sizes were considered and simulations for 20 realizations of both rough surfaces were performed in order to carry out a statistical analysis. The pressure signals near the surface were investigated. The rise time of the front shock is longer for the rough surface configuration. The incoherent part of the field is small compared to the coherent one: a single realization is enough for comparison with experiments because the measurement uncertainties are of the same order as the deviation due to the change of realization. Near the surface, coherent pressure signals obtained for both sets of parameters have a higher maximum than for the smooth surface reference, the increase being of the order of 20%. The pressure variation with the elevations is different for the smooth and the rough cases. The overpressure is almost constant pressure along the Mach stem for the smooth surface, while an exponential decrease is observed for the rough surfaces. These two characteristics of the roughness simulations can be interpreted as a surface wave propagating along the surface. Finally, a preliminary simulation was performed at a larger scale to simulate the reflection of a N-wave over the ground with topographic effects. This demonstrate the feasibility of the study of the sonic boom reflection on the ground.

## ACKNOWLEDGEMENTS

This work has received funding from the EU Horizon2020 programme through the RUMBLE (RegUlation and norM for low sonic Boom LEvels) project under grant agreement no. 769896. It was also supported by RSF-17-72-10277 and by the Labex CeLyA of Universite de Lyon, operated by the French National Research Agency (ANR-10-LABX-0060/ANR-16-IDEX-0005). It was conducted within the framework of LETMA (Laboratoire ETudes et Modélisation Acoustique), a Contractual Research Laboratory shared between CEA, CNRS, Ecole Centrale de Lyon, C-Innov, and Sorbonne Université.

## REFERENCES

- [1] Krehl, P.; Van der Geest, M. The discovery of the Mach reflection effect and its demonstration in an auditorium. *Shock Waves*, 1 (1), pp 3-15, 1991.
- [2] Huber, P. W.; McFarland, D. R. Effect of surface roughness on characteristics of spherical shock waves, NASA Technical Report TR-R-23, pp 1 44, 1959.
- [3] Adachi, T.; Kobayashi, S.; Suzuki, T. An experimental analysis of oblique shock reflection over a two-dimensional multi-guttered wedge, *Fluid Dynamics Research*, Vol 9 (1-3), pp 119-132, 1992.
- [4] Karzova, M.; Lechat, T.; Ollivier, S.; Dragna, D.; Yuldashev, P.; Khokhlova, V.; Blanc-Benon, P. Influence of roughness on nonlinear reflection of weak shock waves, submitted to *JASA Express Letters*.
- [5] Ishimaru, A.; Rockway, J. D.; Lee, S. W. ; Sommerfeld and Zenneck wave propagation for a finitely conducting one-dimensional rough surface. *IEEE Transactions on Antennas and Propagation*, Vol 48 (9), pp 1475-1484, 2000.
- [6] Faure, O.; Gauvreau, B.; Junker, F.; Lafon, P.; Bourlier, C.; Modeling of random ground roughness effects by an effective impedance and application to time-domain methods. *Applied Acoustics*, Vol 119, pp 1-8, 2017.
- [7] Dragna, D.; Blanc-Benon, P.; Poisson, F. Time-domain solver in curvilinear coordinates for outdoor sound propagation over complex terrain. *Journal of the Acoustical Society of America*, Vol 133 (6), pp 3751-3763, 2013.
- [8] Karzova, M. M.; Lechat, T.; Ollivier, S.; Dragna, D.; Yuldashev, P. V.; Khokhlova, V. A.; Blanc-Benon, P. Irregular reflection of spark-generated shock pulses from a rigid surface: Mach-Zehnder interferometry measurements in air. *Journal of the Acoustical Society of America*, Vol 145 (1), pp 26-35, 2019.
- [9] Tripathi, B. B.; Baskar, S.; Coulouvrat, F.; Marchiano, R. Numerical observation of secondary Mach stem in weak acoustic shock reflection. *Journal of the Acoustical Society of America*, 144 (2), EL125-EL130, 2018.
- [10] Maeda, S.; Fujisawa, M.; Ienaga, S.; Hirahara, K.; Obara, T. Effect of sandpaper-like small wall roughness on deflagration-to-detonation transition in a hydrogen-oxygen mixture. *Proceedings of the Combustion Institute*, Vol 37 (3), pp 3609-3616, 2019.
- [11] Bogey, C.; Bailly, C. A family of low dispersive and low dissipative explicit schemes for flow and noise computations. *Journal of Computational Physics*, Vol 194 (1), pp 194-214, 2004.
- [12] Sabatini, R.; Marsden, O.; Bailly, C.; Bogey, C. A numerical study of nonlinear infrasound propagation in a windy atmosphere. *Journal of the Acoustical Society of America*, Vol 140 (1), pp 641-656, 2016.